

1 **Broadband Direct UVA Irradiance Measurement for Clear Skies**
2 **Evaluated Using a Smartphone**

3 **D. Igoe^{1*} & A.V. Parisi¹**

4 ¹Faculty of Health, Engineering and Sciences, University of Southern Queensland,
5 Toowoomba. Australia

6 *Corresponding author: damienspaul@gmail.com

7 Short Title: Broadband Direct UVA Irradiances

8 **Abstract**

9 UVA wavelengths (320-400 nm) have been implicated in recent studies to contribute to
10 melanoma induction and skin photoaging in humans and damage to plants. The use of
11 smartphones in UVA observations are a way to supplement measurements made by
12 traditional radiometric and spectroradiometric technology. Although the smartphone image
13 sensor is not capable of determining broadband UVA irradiances, these can be reconstructed
14 from narrowband irradiances, which the smartphone, with narrowband and neutral density
15 filters, can quantify with discrepancies not exceeding 5%. Three models that reconstruct
16 direct broadband clear sky UVA were developed from narrowband irradiances derived from
17 smartphone image sensor pixel data with coefficients of determination of between 0.97 and
18 0.99. Reasonable accuracy and precision in determining the direct broadband UVA was
19 maintained for observations made with solar zenith angles as high as 70°. The developed
20 method has the potential to increase the uptake of the measurement of broadband UVA
21 irradiances.

22

23 **Introduction**

24 The UVA wavelengths (320-400 nm) are implicated as damaging to human health as possibly
25 contributing to melanoma induction⁽¹⁾. Additionally, the UVA waveband contributes to
26 premature skin aging⁽²⁾. The UVA has also been reported to influence the effects of the UV
27 radiation on damage to plants⁽³⁾. The UVA waveband is also transmitted to varying amounts
28 through glass and plays a role in UV irradiances to humans resulting from UV transmitted
29 through glass⁽⁴⁾. The percentage of transmitted UVA is influenced by the thickness, type of
30 glass and whether or not the glass is laminated or tinted⁽⁵⁻⁸⁾. Critically, the ozone absorption
31 coefficients are significantly less in the UVA compared to the UVB and at 334 nm are 0.8%
32 of that at 297 nm⁽⁹⁾.

33 The techniques of radiometry and spectroradiometry are employed in the measurement of
34 UVA irradiances⁽¹⁰⁾. These include the measurement of the diffuse, direct and global (direct +
35 diffuse) irradiances. The irradiances at the three wavelengths of 320, 340 and 380 nm have
36 been employed in clear sky conditions for the evaluation of solar irradiances⁽¹¹⁾. Another
37 approach to evaluate the UVA irradiances has been the development of a model that employs
38 the measured irradiance at 368 nm and the empirically determined irradiances in the UVA
39 waveband and at 368 nm⁽¹²⁾. Other approaches have employed the use of cloud modification
40 factors to the clear sky irradiances for the evaluation of the UVA^(13,14).

41 The image sensors on smartphones have been reported as having a response in the UVA
42 waveband⁽¹⁵⁾. This quantifiable response has led to the development of a method for
43 evaluation of aerosol optical depth at UVA wavelengths^(16,17). The widespread uptake and use
44 of smartphones has the potential to increase the uptake of the measurement of broadband
45 UVA irradiances. However, in order to achieve this it is necessary to overcome the problem
46 of a smartphone image sensor not being directly capable of measuring broadband UVA due

47 to some phone sensors not possessing a flat response in the UVA. Another limitation is that
48 all phone image sensors respond differently to UV wavelengths. This paper extends the
49 previous research by developing a method for the evaluation of the direct sun, clear sky
50 broadband UVA irradiances with a smartphone.

51

52 **Materials and Methods**

53 The approach employed in this research was to develop a model to evaluate the broadband
54 direct sun UVA irradiances from the direct sun narrowband irradiances measured with a
55 smartphone at 320, 340 and 380 nm. Further data on the direct sun broadband UVA were
56 then collected to validate the model developed against a calibrated ultraviolet meter (model
57 3D, Solar Light, USA). This meter was calibrated for the UVA against a calibrated Bentham
58 spectroradiometer (model DTM300, Bentham Instruments Inc, UK). The input data for the
59 model were the direct sun narrowband UVA irradiances at 320, 340 and 380 nm. These were
60 measured with a LG L3 smartphone (LG Electronics, Seoul, South Korea) image sensor with
61 the image intensity for each measurement calibrated with a Microtops sunphotometer (Model
62 E540, Solar Light, USA) for the narrow band irradiances at the respective wavelengths. This
63 instrument measures the direct sun irradiances at each of the wavelengths with a FWHM of 2
64 nm.

65 *Data for Evaluation of Direct UVA Irradiances*

66 Igoe et al.^(16,17) have demonstrated that there exists a very strong correlation between the
67 natural log of narrow bandwidth irradiances measured by the Microtops and the natural log of
68 the product of the image sensor average grayscale over the same narrow bandwidth, the
69 Earth-sun distance factor and the fourth power of the cosine of the sun zenith angle.

70 The three target narrowband wavelengths employed for this research to evaluate the
71 broadband UVA irradiances were 320 nm, 340 nm and 380 nm. These were selected as they
72 correspond to the narrowband irradiances measured on the Microtops. To ensure that direct
73 solar measurements were made on the smartphone and ultraviolet meter, 7 cm length black
74 tubes of 2.5 cm diameter were used over the respective optics. Narrowband interference
75 filters (Melles Griot, supplier Lastek, Australia) with centre wavelengths of 320, 340 and 380
76 nm respectively and a FWHM of 10 nm were employed on the smartphone to provide the
77 respective wavelengths. These were coupled in a light tight arrangement including the 7 cm
78 black tube with a 1% neutral density filter (Asahi Filters, Tokyo, Japan) to prevent the
79 saturation of the image sensor^(16,17). Additionally, an ND2 neutral density filter (Bentham
80 Instruments, Inc. UK) was used for 380 nm observations due to the higher irradiance at this
81 waveband^(16,17).

82 Direct sun measurements were performed at 20 minute intervals, between 9:00 am and noon
83 on cloud free days, from late May to late June on a high school oval in Gladstone,
84 Queensland (23.91°S 151.27°E) with a solar zenith angle range of 67° to 47°. Two sets of
85 observations were made, three weeks apart to obtain the data to develop the model for the
86 evaluation of the direct UVA irradiances. The atmospheric ozone range was 262 to 294 DU.
87 The aerosol optical depth ranged from 0.16 to 0.21 and 0.06 to 0.09 at 340 and 380 nm
88 respectively.

89 The smartphone and ultraviolet meter sensors were oriented in the same direction as that of
90 the Microtops, using the sun alignment optics on the sun photometer to ensure all three
91 instruments recorded direct sun irradiances for each measurement. The data recorded include
92 the image data from the smartphone image sensor with 3 images of the direct sun at each of
93 320, 340 and 380 nm taken at each measurement time, the irradiances recorded at 320 nm,
94 340 nm and 380 nm; aerosol optical depth at 340 nm and 380 nm and solar zenith angle from

95 the Microtops and the total direct UVA irradiances from the ultraviolet meter. Each set of
96 measurements were taken within 5 minutes, with minimal change in the UVA irradiances
97 over that time of the order of less than 4% at 9 am and less than 1% at noon.

98 A previously described smartphone app that was written to determine the mean and standard
99 deviation of the grayscale (intensity) response detected by the image sensor above a dark
100 noise threshold⁽¹⁷⁾ was employed, where the grayscale was calculated using:

$$101 \quad \textit{Grayscale} = 0.299(\textit{red}) + 0.587(\textit{green}) + 0.114(\textit{blue}) \quad (1)$$

102 The terms red, green and blue are the average of the pixel values in the respective
103 channels⁽¹⁸⁾. Recent studies by Igoe et al.⁽¹⁹⁾, demonstrated that the magnitude of thermally-
104 induced dark noise does not vary significantly through daytime temperatures; hence can be
105 considered as a constant threshold. Average grayscale responses were taken above the dark
106 noise threshold, over the solar disk.

107 *Model Development and Evaluation*

108 The ultraviolet meter total direct UVA was compared to the sum of smartphone-derived
109 irradiances ($I_{320} + I_{340} + I_{380}$) where each of the terms is the irradiances at each of 320, 340
110 and 380 nm respectively. Additionally, the broadband UVA was compared to the irradiances
111 for each wavelength individually, in a similar manner to Grant and Slusser⁽¹²⁾ to determine if
112 any wavelength (or their sum) would provide an accurate model for broadband direct sun
113 UVA. Another model tested was to use the trapezoidal method in determining the relative
114 irradiance proportions each narrowband wavelength contributes to the broadband direct sun
115 UVA. The sum therefore becomes $10I_{320} + 30I_{340} + 40I_{380}$, this model is denoted as I_{trap} .

116 Once calibrations and development of the model were complete over two trial days,
117 verification tests were performed to validate the accuracy and precision of the broadband

118 direct sun UVA model developed in conditions where the AOD were different. This data
119 were collected on relatively cloud free days on the 29th June and 7th July 2014 between 8 am
120 and noon with a solar zenith angle range of 70° to 44°. The atmospheric ozone range was 267
121 to 291 DU and the average aerosol optical depth range was 0.15 and 0.05 for 340 nm and 380
122 nm respectively.

123

124 **Results and Discussion**

125 The smartphone image sensor was first calibrated to each of the natural log of the direct sun
126 irradiances recorded by the Microtops at 320 nm, 340 nm and 380 nm. The calibration
127 followed the general approach established by Igoe et al.⁽¹⁶⁾ experimentally and used in an app
128 to detect aerosol optical depth⁽¹⁷⁾. The general relationship between the natural log of direct
129 irradiance from the Microtops ($I_{Microtops}$) to the ‘cosine grey’ value derived from the average
130 of the grayscale values (Y_{av}) above a threshold from the smartphone is presented below. This
131 value represents the average over approximately 1600 pixels in each image and averaged
132 over three images.

$$133 \quad \ln I_{Microtops} = m \ln(Y_{av} D^2 \cos^4 SZA) + c \quad (2)$$

134 where D^2 represents the Sun-Earth distance correction factor⁽²⁰⁾, SZA is the solar zenith angle
135 and m and c are the correlation gradient and intercept respectively.

136 The correlations between the Microtops and smartphone derived values were very strong for
137 all three target wavelengths, with coefficients of determination of 0.99, 0.99 and 0.97 for 380
138 nm, 340 nm and 320 nm observations respectively where the x axis values of smartphone
139 cosine grey are $\ln(Y_{av} D^2 \cos^4 SZA)$.

140

141 A source of variation for the UVA irradiances is the aerosol optical depth. The calibration
142 observations were made on days with different aerosol optical depths, as measured by the
143 Microtops. These were 0.189 ± 0.013 and 0.075 ± 0.006 for 340 nm and 380 nm respectively.
144 Another source of variation is the differences in the image sensors between different phones
145 and different models. In a similar manner to how individual UV radiometers need calibration,
146 individual phone image sensors will require calibration.

147 The smartphone derived direct sun UVA irradiances for each of the models were compared to
148 the direct sun UVA irradiances measured with the meter. The coefficient of determination of
149 broadband direct sun UVA comparisons varied considerably with wavelength (Table 1). For
150 practicality, each regression was set to have an intercept of zero to better describe the
151 relationship between broadband direct sun UVA and smartphone derived narrowband
152 irradiances.

153 >Table 1<

154 The very strong correlation observed for the model bases I_{380} , $(I_{320} + I_{340} + I_{380})$ and I_{trap}
155 suggest that any of these could be used as a proxy to model the total direct clear sky UVA
156 irradiances using smartphone image sensor derived irradiances, the derived regressions for
157 the LG L3 smartphone are in equations 3, 4 and 5 and the regression lines are in Figures 1, 2
158 and 3 respectively.

$$159 \quad UVA_{direct} = 12.01I_{380} \quad (3)$$

$$160 \quad UVA_{direct} = 8.95(I_{320} + I_{340} + I_{380}) \quad (4)$$

$$161 \quad UVA_{direct} = 0.25I_{trap} \quad (5)$$

162 >Figure 1<

163 >Figure 2<

164 >Figure 3<

165

166 The results for evaluation of broadband UVA were validated on clear sky days where the
167 AOD was less than that observed in the calibration phase, recording averages of 0.152 ± 0.013
168 and 0.049 ± 0.002 for 340 nm and 380 nm respectively. When the validation data was
169 modelled with the calibration data and compared to the direct sun UVA detected by the
170 ultraviolet meter, there were no measurable effects of the lower AOD. Additionally, six
171 measurements were taken at SZAs of over 60° , including as high as 70° (air mass 2.92) and
172 exhibited no significant discrepancies, as shown in Figures 4 to 6.

173

174 >Figure 4<

175

176 >Figure 5<

177

178 >Figure 6<

179

180 Discrepancies between the direct sun UVA models and values recorded by the ultraviolet
181 meter typically were within approximately 4%, increasing as the solar zenith angle increased
182 beyond 60° . The three models demonstrated similar precision in determining direct UVA
183 irradiances (Figure 7). The model based on I_{380} is easier to implement in terms of the input

184 data required. This model should be applicable for the clear sky cases where there are not
185 significant variations in the relative shape of the UVA spectrum. The other two models that
186 include I_{320} and I_{340} take into account variations in the relative shape of the UVA spectrum.

187 >Figure 7<

188

189 **Conclusion**

190 A method has been developed and validated to evaluate the direct sun clear sky irradiances
191 from narrowband direct sun smart phone derived images. Three accurate and precise models
192 were employed to reconstruct the direct sun broadband UVA clear sky irradiances from
193 narrowband irradiance observations made using a smartphone image sensor. Narrowband
194 irradiances were calibrated against standard instrumentation. Additional calibration was
195 made using an ultraviolet meter to reconstruct the direct sun UVA clear sky irradiances.
196 Calibration and validation observations demonstrated that the reconstruction provides reliable
197 direct sun, clear sky UVA irradiances at solar zenith angles up to 67° . The developed method
198 has the potential to increase the uptake of the measurement of broadband UVA irradiances.
199 Examples of where they can be utilised are in schools for both the teaching of physics
200 principles and for the education of children about solar radiation.

201

202 **References**

203

- 204 1. Noonan, F. P., Zaidi, M. R., Wolnicka-Glubisz, A., Anver, M. R., Bahn, J., Wielgus.
205 A., Cadet, J., Douki, T., Mouret, S., Tucker, M. A., Popratiloff, A., Merlino, G., De
206 Fabo, E. C., Melanoma induction by ultraviolet A but not ultraviolet B radiation
207 requires melanin pigment. *Nature Communications*, 3:884 doi: 10.1038/ncomms1893
208 (2012).
- 209 2. McCullough, J. L. and Kelly, K. M. Prevention and treatment of skin ageing. *Annals*
210 *NY Acad. Sci.* 1067, 323-331 (2006).
- 211 3. Flint, S. D. and Caldwell, M. M. A biological spectral weighting function for ozone
212 depletion research with higher plants. *Physiol. Plant*, 117, 137-144 (2003).
- 213 4. Wong, C. F. and Parisi, A. V. Measurement of UVA exposure to solar radiation.
214 *Photochem. Photobiol.* 63, 807-810 (1996).
- 215 5. Duarte, I., Rotter, A., Malvestiti, A. and Silva, M. The role of glass as a barrier
216 against the transmission of ultraviolet radiation: an experimental study.
217 *Photodermatol. Photoimmunol. Photomed*, 25, 181-184 (2009).
- 218 6. Almutawa, F. and Buabbas, H. Photoprotection clothing and glass. *Dermatol. Clin.*
219 32, 439-448 (2014).
- 220 7. Parisi, A. V., Turnbull, D. J. and Kimlin, M. G. Dosimetric and spectroradiometric
221 investigations of glass filtered solar UV. *Photochem. Photobiol.* 83, 777-781 (2007).
- 222 8. Hampton, P. J., Farr, P. M., Diffey, B. L. and Lloyd, J. J. Implication for
223 photosensitive patients of ultraviolet A exposure in vehicles. *Br. J. Dermatology*, 151,
224 873-876 (2004).

- 225 9. Daumont, D., Brion, J., Charbonnier, J & Malicet, J. Ozone UV spectroscopy I:
226 Absorption cross-sections at room temperature. *J. Atmospheric Chemistry*, 15, 145-
227 155 (1992).
- 228 10. Diffey, B. L. Sources and measurement of ultraviolet radiation. *Methods*, 28, 4-13,
229 (2002).
- 230 11. Anav, A., Rafanelli, C., Di Menno, I. and Di Menno, M. An algorithm to evaluate
231 solar irradiance and effective dose rates using spectral UV irradiance at four selected
232 wavelengths. *Rad. Prot. Dosim.* 111, 239-250 (2004).
- 233 12. Grant, R. and Slusser, J. Estimation of ultraviolet-A irradiance from measurement of
234 368 nm spectral irradiance. *J. Atm. Ocean. Tech.* 22, 1853-1863 (2005).
- 235 13. Jacovides, C. P., Tymvios, F. S., Assimakopoulos, V. D., Kaltsounides, N. A.,
236 Theoharatos, G. A. and Tsitouri, M. Solar global UVB (280-315 nm) and UVA (315-
237 380 nm) radiant fluxes and their relationships with broadband global radiant flux at an
238 eastern Mediterranean site. *Agric. For. Meteorol.* 149, 1188-1200 (2009).
- 239 14. Parisi, A. V., Downs, N. and Turner, J. Evaluation of the cloudy sky solar UVA
240 radiation exposures. *J. Photochem. Photobiol. B: Biol.* 138, 141-145 (2014).
- 241 15. Igoe, D., Parisi, A. V. and Carter, B. Characterisation of the UVA response of a smart
242 phone. *Photochem. Photobiol.* 89, 215-218 (2013).
- 243 16. Igoe, D., Parisi, A. V. and Carter, B. Evaluating UVA aerosol optical depth using a
244 smartphone camera. *Photochem. Photobiol.* 89, 1244-1248 (2013).
- 245 17. Igoe, D., Parisi, A. V. and Carter, B. Smartphone-based Android app for determining
246 UVA aerosol optical depth and solar irradiances. *Photochem. Photobiol.* 90, 233-237
247 (2014).
- 248 18. Malacara, D. *Color Vision and Colorimetry: Theory and Applications*. Bellingham,
249 SPIE Press (2002).

250 19. Igoe, D., Parisi, A. V. and Carter, B. A method for determining the dark response for
251 scientific imaging with smartphones. *Instrumentation Science and Technology*, 42,
252 586-592 (2014).

253 20. Morys, M., Mims III, F., Hagreup, S., Anderson, S., Baker, A., Kia, J. and Walkup, T.
254 Design, calibration, and performance of MICROTOPS II handheld ozone monitor and
255 sun photometer. *J. Geophys. Res.* 106, 14573-14582 (2001).

256

257

258

259

260

261

262

263

264

265

266 **Tables**

267

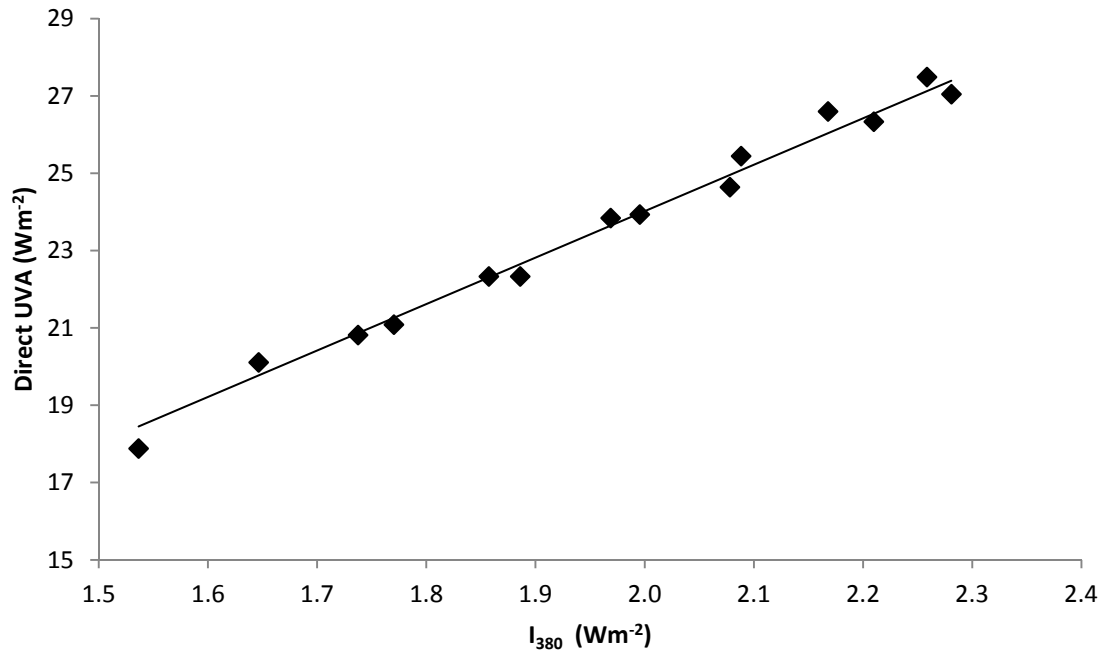
268 Table 1: Coefficient of determination of narrowband wavelength based models for broadband
269 direct sun UVA irradiances.

270

<i>Model base</i>	<i>R²</i>
I ₃₂₀	0.127
I ₃₄₀	0.819
I ₃₈₀	0.987
I ₃₂₀ + I ₃₄₀ + I ₃₈₀	0.968
I _{trap}	0.984

271

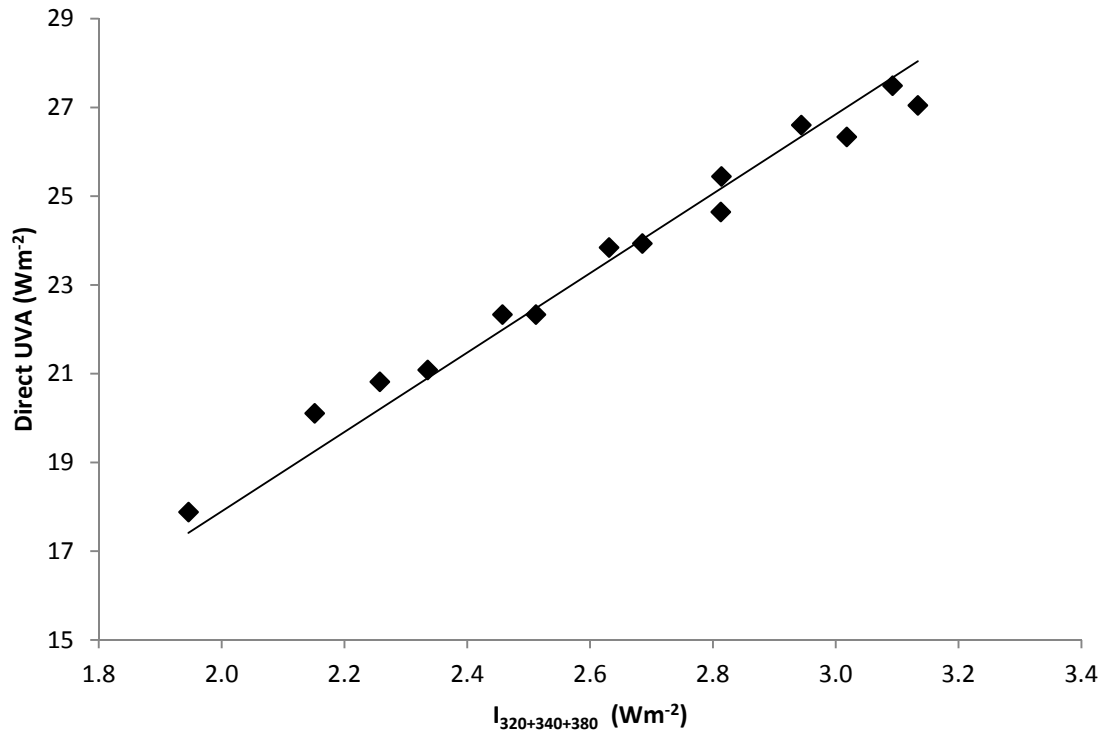
272



273

274 Figure 1: Model for the determination of the broadband direct sun UVA irradiances from the
275 smartphone derived narrowband direct sun irradiances at 380 nm.

276

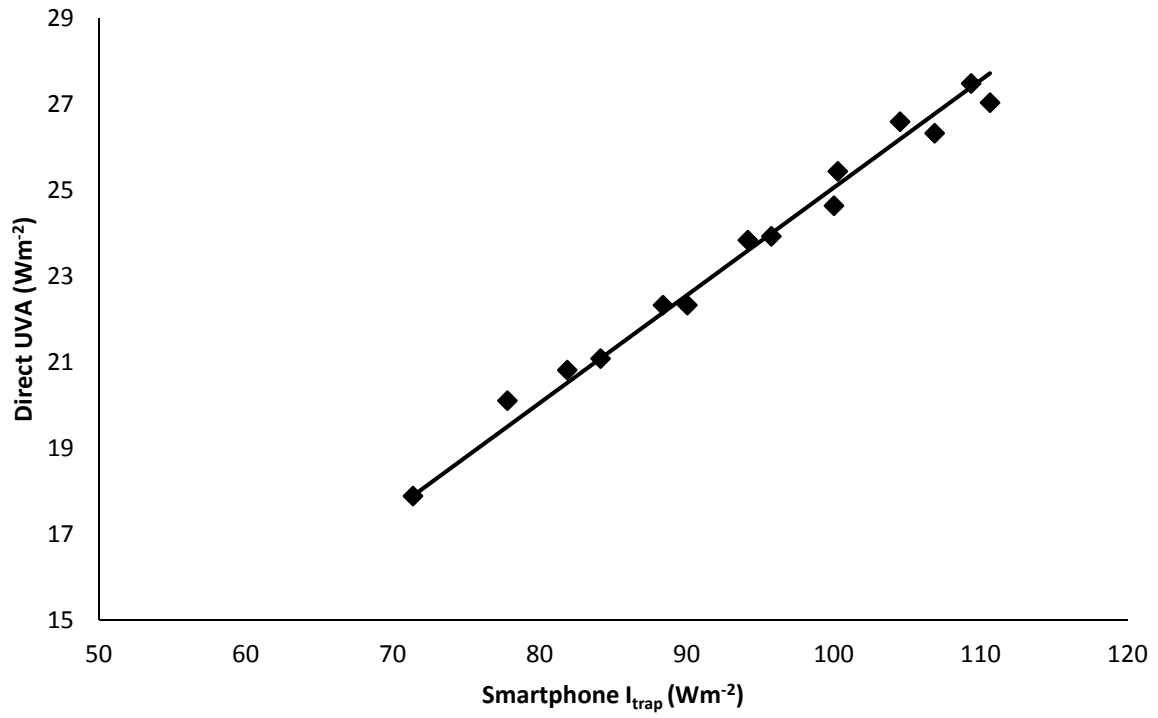


277

278 Figure 2: Model for the determination of the broadband direct sun UVA irradiances from the

279 sum of the smartphone derived narrowband direct sun irradiances at 320, 340 and 380 nm.

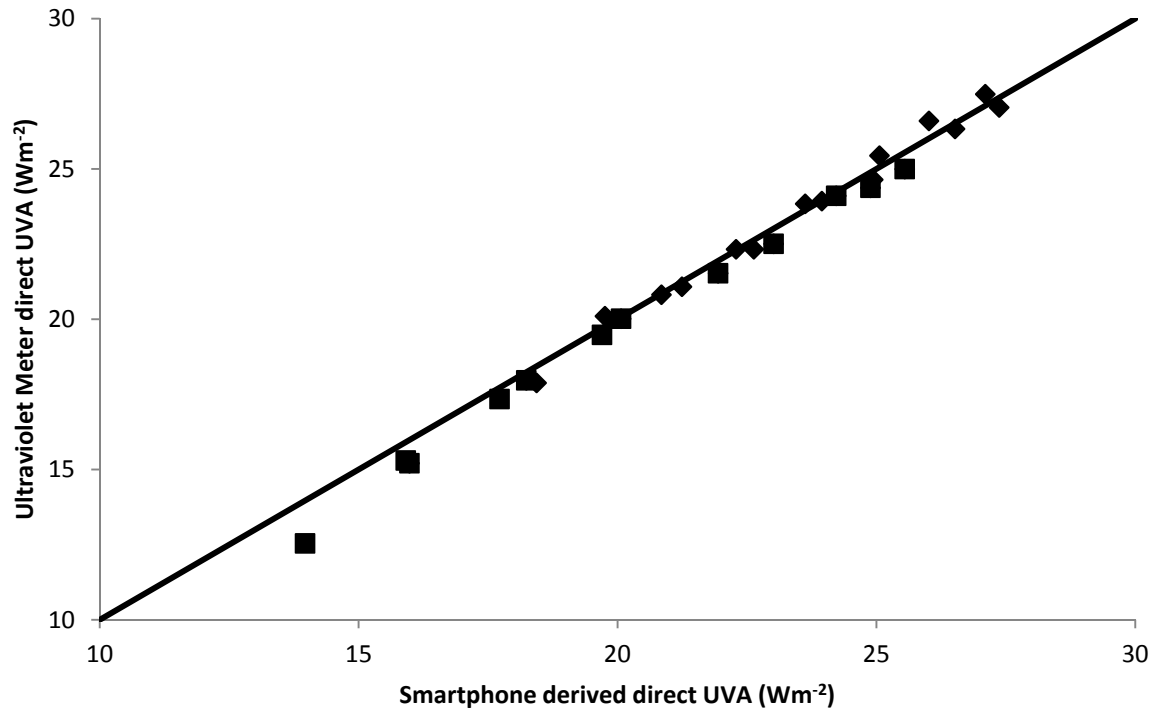
280



281

282 Figure 3: Model for the determination of the broadband direct sun UVA irradiances from the
 283 smartphone derived narrowband direct sun irradiances using $(10 \times I_{320} + 30 \times I_{340} + 40 \times I_{380})$.

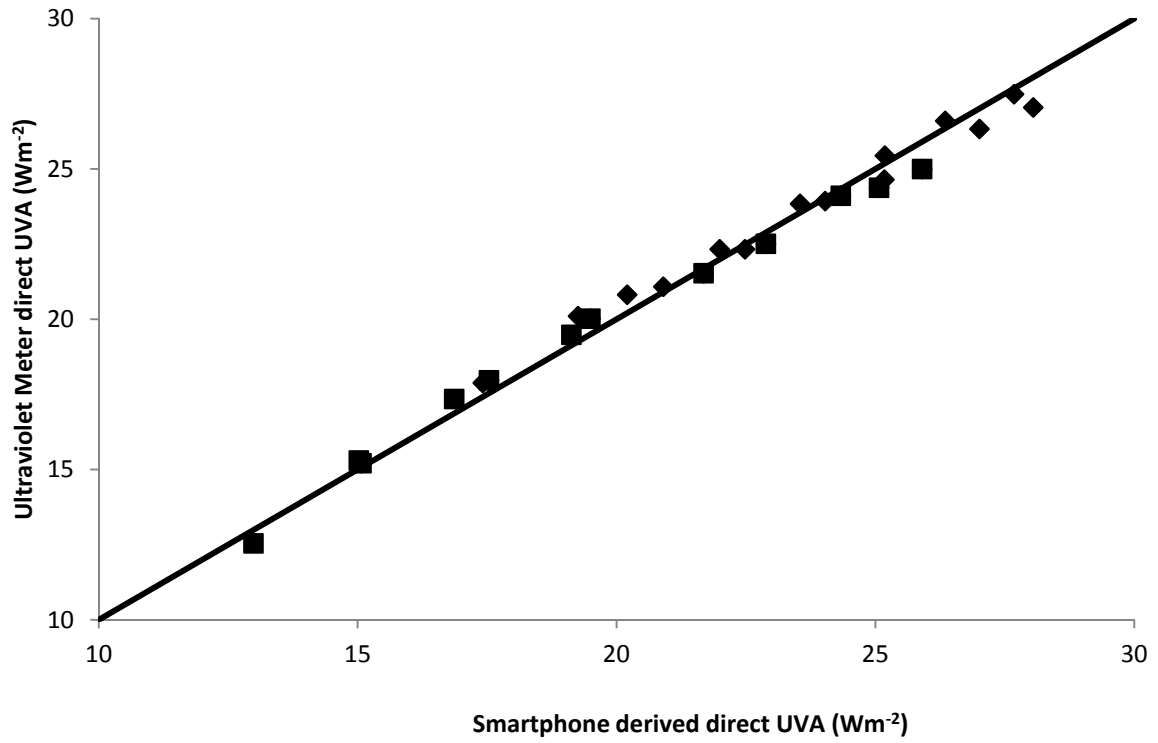
284



285

286 Figure 4: Comparison of smartphone derived direct sun UVA irradiances with corresponding
 287 measurements from the ultraviolet meter for validation data with the I_{380} model applied. The
 288 boxes and diamonds represent the validation and calibration data respectively and the line
 289 represents an exact match.

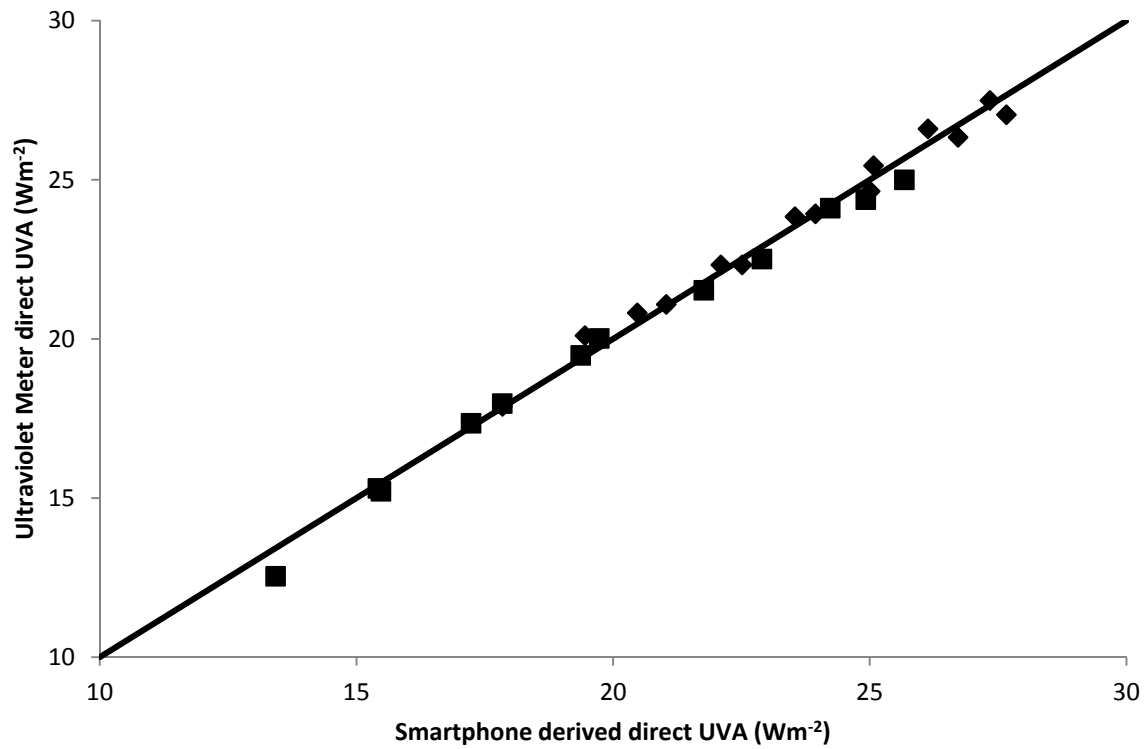
290



291

292 Figure 5: Comparison of smartphone derived direct sun UVA irradiances with corresponding
 293 measurements from the ultraviolet meter for validation data with the $(I_{320} + I_{340} + I_{380})$
 294 model applied. The boxes and diamonds represent the validation and calibration data
 295 respectively and the line represents an exact match.

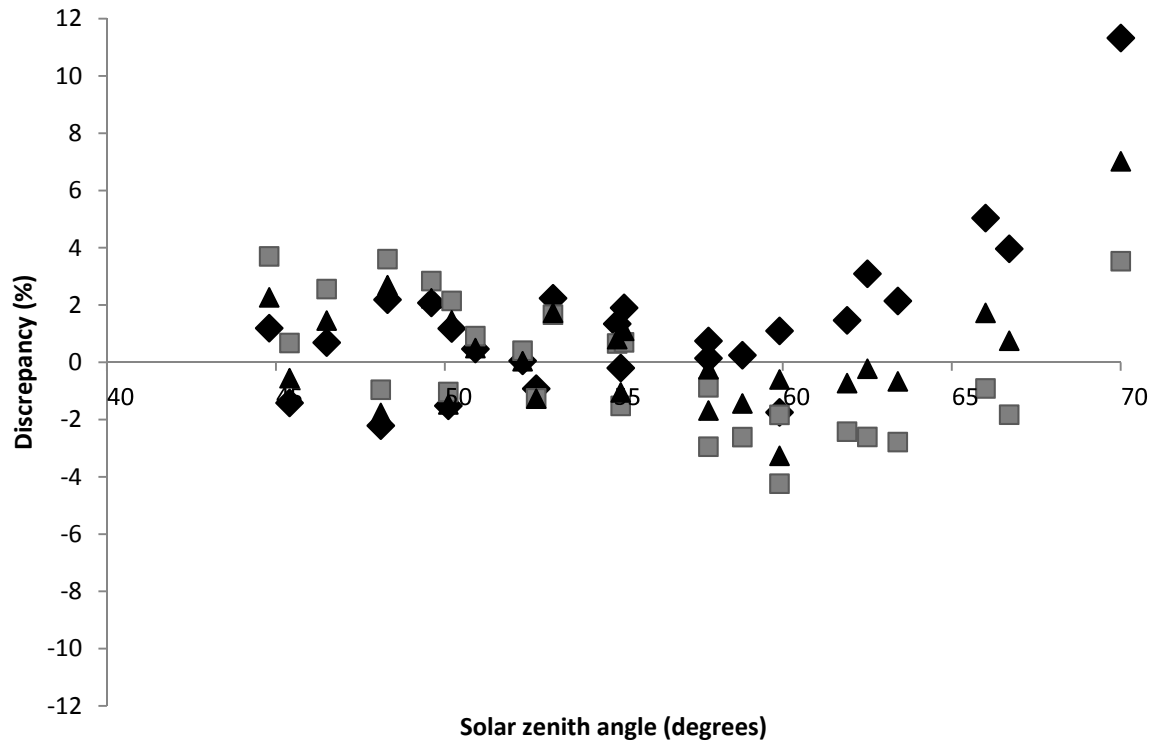
296



297

298 Figure 6: Comparison of smartphone derived direct sun UVA irradiances with corresponding
 299 measurements from the ultraviolet meter for validation data with the I_{trap} model applied. The
 300 boxes and diamonds represent the validation and calibration data respectively and the line
 301 represents an exact match.

302



303

304 Figure 7: Comparison of percentage discrepancies between the modelled broadband direct
 305 sun UVA and observations made by the ultraviolet meter. Diamonds represent the I₃₈₀
 306 model, squares represent the (I₃₈₀ + I₃₄₀ + I₃₂₀) model and the triangles represent the I_{trap}
 307 model.

308